



HAL
open science

Mineralogical Investigation of Mg-Sulfate at the Canaima Drill Site, Gale Crater, Mars

S. J. Chipera, D. T. Vaniman, E. B. Rampe, T. F. Bristow, G. Martínez, V.
M. Tu, T. S. Peretyazhko, A. S. Yen, R. Gellert, J. A. Berger, et al.

► **To cite this version:**

S. J. Chipera, D. T. Vaniman, E. B. Rampe, T. F. Bristow, G. Martínez, et al.. Mineralogical Investigation of Mg-Sulfate at the Canaima Drill Site, Gale Crater, Mars. *Journal of Geophysical Research. Planets*, 2023, 128, 10.1029/2023JE008041 . insu-04473134

HAL Id: insu-04473134

<https://insu.hal.science/insu-04473134>

Submitted on 23 Feb 2024

HAL is a multi-disciplinary open access archive for the deposit and dissemination of scientific research documents, whether they are published or not. The documents may come from teaching and research institutions in France or abroad, or from public or private research centers.

L'archive ouverte pluridisciplinaire **HAL**, est destinée au dépôt et à la diffusion de documents scientifiques de niveau recherche, publiés ou non, émanant des établissements d'enseignement et de recherche français ou étrangers, des laboratoires publics ou privés.



Distributed under a Creative Commons Attribution 4.0 International License

Mineralogical Investigation of Mg-Sulfate at the Canaima Drill Site, Gale Crater, Mars



Key Points:

- For the first time on Mars, starkeyite ($\text{MgSO}_4 \cdot 4\text{H}_2\text{O}$) was positively identified
- Starkeyite along with amorphous $\text{MgSO}_4 \cdot n\text{H}_2\text{O}$ are the “polyhydrated Mg-sulfates” interpreted in orbital reflectance spectra
- Mg-sulfate mineralogy serves as an indicator of transition to a drier climate and helps outline the climatic and depositional changes on Mars













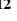




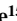


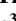



Correspondence to:

S. J. Chipera,
Steve.Chipera@gmail.com

Citation:

Chipera, S. J., Vaniman, D. T., Rampe, E. B., Bristow, T. F., Martínez, G., Tu, V. M., et al. (2023). Mineralogical investigation of Mg-sulfate at the Canaima drill site, Gale crater, Mars. *Journal of Geophysical Research: Planets*, 128, e2023JE008041. <https://doi.org/10.1029/2023JE008041>

Received 3 AUG 2023
Accepted 10 OCT 2023

S. J. Chipera¹ , D. T. Vaniman¹ , E. B. Rampe² , T. F. Bristow³ , G. Martínez⁴ , V. M. Tu⁵, T. S. Peretyazhko⁵ , A. S. Yen⁶ , R. Gellert⁷, J. A. Berger⁵, W. Rapin⁸, R. V. Morris² , D. W. Ming², L. M. Thompson⁹ , S. Simpson² , C. N. Achilles¹⁰ , B. Tutolo¹¹ , R. T. Downs¹² , A. A. Fraeman⁶ , E. Fischer¹³ , D. F. Blake³, A. H. Treiman⁴ , S. M. Morrison¹⁴ , M. T. Thorpe¹⁵ , S. Gupta¹⁶, W. E. Dietrich¹⁷, G. Downs¹⁸, N. Castle¹ , P. I. Craig¹ , D. J. Des Marais³ , R. M. Hazen¹⁴ , A. R. Vasavada⁶ , E. Hausrath¹⁹ , P. Sarrazin²⁰, and J. P. Grotzinger²¹

¹Planetary Science Institute, Tucson, AZ, USA, ²NASA Johnson Space Center, Houston, TX, USA, ³NASA Ames Research Center, Moffett Field, CA, USA, ⁴Lunar and Planetary Institute/USRA, Houston, TX, USA, ⁵Jacobs JETSIL, NASA Johnson Space Center, Houston, TX, USA, ⁶Jet Propulsion Laboratory, California Institute of Technology, Pasadena, CA, USA, ⁷Department of Physics, University of Guelph, Guelph, ON, Canada, ⁸Institut de Recherche en Astrophysique et Planétologie, Université de Toulouse 3 Paul Sabatier, CNRS, CNES, Toulouse, France, ⁹Earth Sciences, University of New Brunswick, Fredericton, NB, Canada, ¹⁰NASA Goddard Space Flight Center, Greenbelt, MD, USA, ¹¹Earth, Energy, and Environment Department, University of Calgary, Calgary, AB, Canada, ¹²Department of Geosciences, University of Arizona, Tucson, AZ, USA, ¹³Department of Climate and Space Sciences and Engineering, University of Michigan, Ann Arbor, MI, USA, ¹⁴Earth and Planets Laboratory, Carnegie Institution for Science, Washington, DC, USA, ¹⁵University of Maryland, NASA Goddard Space Flight Center, Greenbelt, MD, USA, ¹⁶Imperial College London, South Kensington Campus, London, UK, ¹⁷Department of Earth and Planetary Science, University of California Berkeley, Berkeley, CA, USA, ¹⁸Computer Science Department, Stanford University, Stanford, CA, USA, ¹⁹Department of Geoscience, University of Nevada, Las Vegas, NV, USA, ²⁰eXaminArt, Mountain View, CA, USA, ²¹Division of Geological and Planetary Sciences, California Institute of Technology, Pasadena, CA, USA

Abstract For the first time on Mars, the crystalline magnesium-sulfate mineral starkeyite ($\text{MgSO}_4 \cdot 4\text{H}_2\text{O}$) was definitively identified using the CheMin X-ray diffraction instrument at Gale crater. At the Canaima drill site, starkeyite along with amorphous $\text{MgSO}_4 \cdot n\text{H}_2\text{O}$ are among the “polyhydrated Mg-sulfates” interpreted in orbital reflectance spectra. Mg-sulfates are good climate indicators as they are very responsive to changes in temperature and relative humidity. We hypothesize that, through evaporation, Mg-sulfates formed at the end of brine evolution when ion concentrations became saturated and precipitated on the surface or near sub-surface as either epsomite or meridianiite. These minerals were subsequently dehydrated later to starkeyite and amorphous $\text{MgSO}_4 \cdot n\text{H}_2\text{O}$ in response to a drier Mars. At Canaima, starkeyite is stable and would form during the warmer Mars summers. Due to very slow kinetics at the low Mars winter temperatures, starkeyite and amorphous $\text{MgSO}_4 \cdot n\text{H}_2\text{O}$ would be resistant to recrystallize to more hydrous forms and thus likely persist year-round. During the course of analyses, starkeyite transforms into amorphous $\text{MgSO}_4 \cdot n\text{H}_2\text{O}$ inside the rover body due to the elevated temperature and greatly reduced relative humidity compared to the martian surface at the Canaima drill site. It is possible that crystalline sulfate minerals existed in earlier samples measured by CheMin but altered inside the rover before they could be analyzed. Starkeyite is most likely prevalent in the subsurface, whereas both starkeyite and amorphous $\text{MgSO}_4 \cdot n\text{H}_2\text{O}$ are likely present on the surface as starkeyite could partially transform into amorphous $\text{MgSO}_4 \cdot n\text{H}_2\text{O}$ due to direct solar heating.

Plain Language Summary For the first time on Mars, starkeyite ($\text{MgSO}_4 \cdot 4\text{H}_2\text{O}$), one of the many possible naturally occurring Mg-sulfate minerals, has been identified using instruments that determine the mineralogy and chemistry of samples on the *Curiosity* rover in Gale crater. Minerals form in response to conditions they are subjected to and can be used to infer temperature, pressure, water availability, and other factors that will influence their formation. As such, their presence can be used to help define current and past climate conditions on Mars. When Mg-sulfate minerals first precipitate from brine that is evaporating on the surface, they form more hydrous varieties. In response to drier conditions, they will recrystallize to Mg-sulfate forms with less water in them. When Mg-sulfate minerals are desiccated under extremely dry conditions, they will lose their crystal structure and form an amorphous phase. This occurred inside the rover body during the analysis of the Canaima sample. It is likely that earlier samples may also have contained crystalline Mg-sulfates but altered to an amorphous phase while in the rover body before analyses could take place. Mg-sulfate in the subsurface is likely starkeyite but could partially transform on the surface to amorphous $\text{MgSO}_4 \cdot n\text{H}_2\text{O}$ due to direct solar heating.

© 2023. The Authors.

This is an open access article under the terms of the [Creative Commons Attribution License](https://creativecommons.org/licenses/by/4.0/), which permits use, distribution and reproduction in any medium, provided the original work is properly cited.

1. Introduction

The Mars Science Laboratory (MSL) *Curiosity* rover landed in Gale crater on 6 August 2012. Its mission objective is to evaluate habitability on early Mars, in part by elucidating the role of water in martian geologic evolution and characterizing the sedimentary record of early Mars. As part of its instrument suite, *Curiosity* carries CheMin (CHEmistry/MINeralogy), the first X-ray Diffraction (XRD) instrument to be deployed on another planet. CheMin uses X-ray crystallography to directly identify mineral phases and X-ray amorphous components in soil and rock samples (Blake et al., 2012). For more than a decade, CheMin has been returning quantitative mineralogical and corresponding mineral-chemistry data from ~3.5-billion-year-old (Ga) sedimentary rocks, mostly derived from basaltic sources, in Gale crater (Figure 1a). These samples chronicle the mineralogy and sedimentary history of more than 600 vertical meters of lacustrine, fluvial, and Aeolian sediments that comprise the lower strata of the central mound of Gale crater (Aeolis Mons; informally known as Mount Sharp) and the surrounding plains (Aeolis Palus). Recently, *Curiosity* transited from the “phylosilicate-rich unit” into the “Mg-sulfate-bearing unit,” a long-anticipated region of Mount Sharp marked by orbital near-IR detections of hydrated magnesium sulfate minerals by NASA’s Mars Reconnaissance Orbiter (MRO) years before *Curiosity*

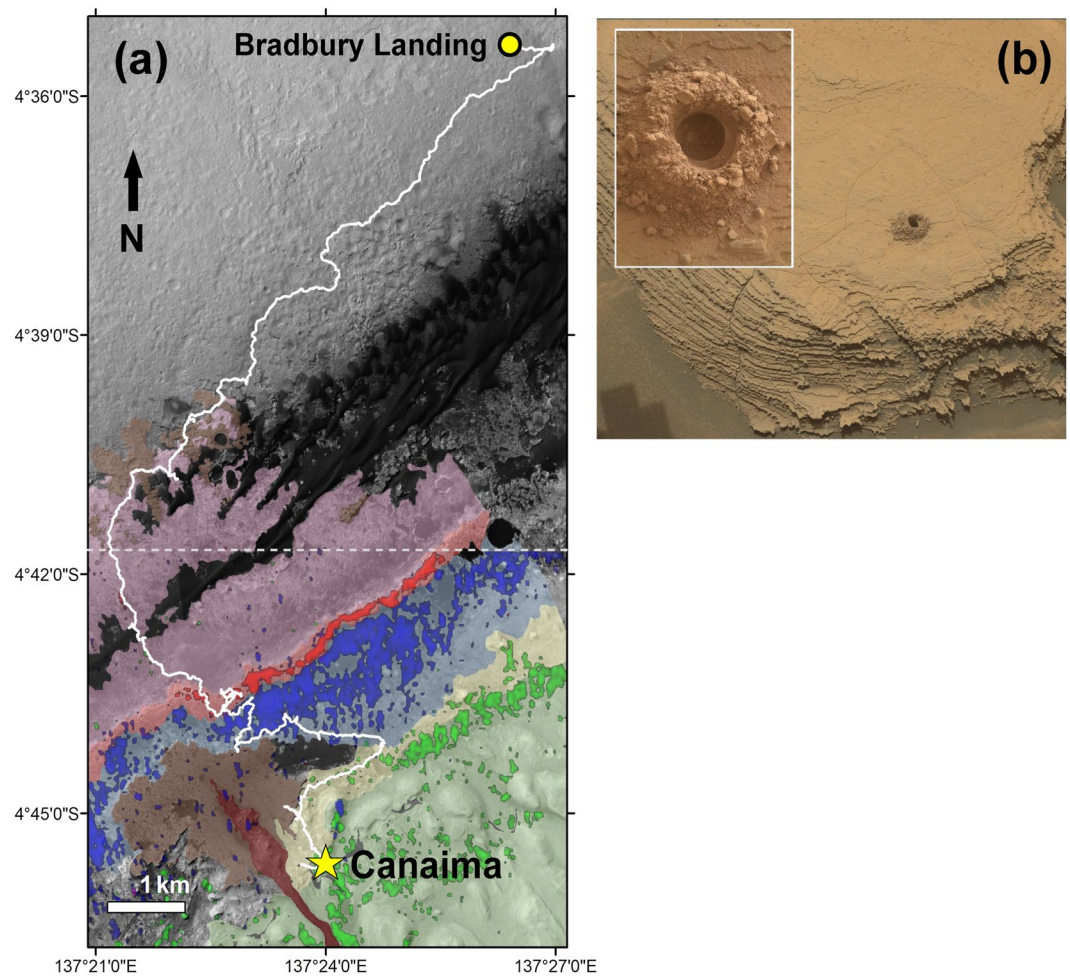


Figure 1. (a) MSL traverse (white line) from its landing site through strata heading southwest across the Gale crater plains toward the base of Mount Sharp, then heading south/southeast up the lower slopes. White horizontal dashed line delineates a boundary north of which only limited CRISM data exist. Red, blue, and green colors show where orbital spectra are interpreted to indicate hematite (Vera Rubin ridge), phyllosilicate (Glen Torridon), and polyhydrated Mg-sulfate, respectively. The yellowish-green area is a transitional zone between clay-bearing and Mg-sulfate-bearing units. Mineralogy inferred from orbital data is described in Fraeman et al. (2013), Milliken et al. (2010), and Sheppard et al. (2021). Image credit: NASA/JPL-Caltech. (b) Mastcam image showing the Canaima drill target with inset image of the drill hole as viewed by the Mars Hand Lens Imager (MAHLI). The drill hole is 1.6 cm wide. Image credit: NASA/JPL-Caltech/MSSS.

landed (Milliken et al., 2010). The first sample obtained from the Mg-sulfate-bearing unit and the mission's 36th drill sample is a rock named “Canaima” (Figure 1b).

In February 2021, *Curiosity* explored a region of Gale crater below the Canaima drill site named Glen Torridon (Figure 1a) that contained fluvio-lacustrine sedimentary layers with abundant Fe³⁺-bearing dioctahedral smectite (i.e., nontronite) (Bristow et al., 2021; Thorpe et al., 2022). Above the clay-bearing strata, the sedimentary succession contains weak signatures of hydrated Mg-sulfate in orbital reflectance spectroscopy (Milliken et al., 2010; Sheppard et al., 2021) and is termed the clay-sulfate transition. Bedrock in the lower part of the succession is overprinted by diagenetic features that obscure primary sedimentary structures, but higher up in the succession, large-scale trough cross-stratified sandstones are present and interpreted to be formed in an aeolian environment (Rapin et al., 2021). Above these sandstones, there is a transition into pervasively planar laminated facies in an area informally named Marker Band Valley that is designated as the Catrimani member of the Mirador formation. The Canaima drill sample (Figure 1b) was drilled into rocks near the base of the Catrimani member that consisted of plane-parallel laminated strata of indeterminate grain size but considered likely to be sandstones. Planar stratification is interpreted to be “pinstripe” lamination formed by migration of aeolian wind ripples (e.g., Fryberger & Schenk, 1988) and suggests that these ripples formed in an aeolian sandsheet environment. After the cessation of the sediment deposition that built Mount Sharp, an extended period of wind-swept erosion occurred. Perhaps in the Hesperian or early Amazonian, after extensive erosion when Canaima was about 80 m below the ground surface, runoff into Gale crater built a lake that would have been about 500 m deep, with a shoreline in the vicinity of Canaima, and appears to have been followed by at least two successive crater lakes (Palucis et al., 2016).

2. Materials and Methods

2.1. CheMin XRD Analyses

Drill powder from Canaima was delivered to CheMin on sol 3614 (sol number is a martian day incrementing since landing on the surface) and analyzed for a total of 22 hr over three separate overnight analyses. CheMin collects X-ray diffraction (XRD) and X-ray fluorescence (XRF) data simultaneously using Co radiation in transmission geometry (a detailed instrument description can be found in Blake et al., 2012). The Canaima sample was obtained using the MSL drill, and ~50 mm³ volume was delivered to a CheMin analysis cell with Kapton windows. During analysis, the cell was shaken piezoelectrically to randomize grain orientations, presenting all lattice orientations to the incident Co X-rays (Sarrazin et al., 2005). A charge-coupled device (CCD) detector was used to determine the energy of photons striking the CCD; fluoresced photons provided XRF data and the two-dimensional (2D) positions of diffracted Co K α photons are used to construct the diffraction pattern. Circumferential integration of the Debye diffraction rings, adjusted for arc length, produced a conventional 1D XRD pattern from 2 to 52°2 θ with an instrumental peak resolution of ~0.3°. Positions of diffracted photons are summed over repeated 10-s measurements for several hours during each night of analysis. CheMin operates at night at the lowest possible temperature. This is necessary because acceptable cold operating temperature for energy discrimination by the CCD detector can only be reached at night when the heat load from the rover deck is minimal. Plagioclase is a common phase in almost all samples, and the 1D diffraction patterns are corrected for minor variations in sample-to-detector distance using the best fit to plagioclase *c* and γ cell parameters (Morrison, Downs, Blake, Prabhu, et al., 2018).

2.2. XRD Data Analysis

For analyses of CheMin X-ray diffraction data, the abundances of phases were determined using both Rietveld and full-pattern fitting methods. Rietveld refinement (conducted with JADE from Materials Data Inc.) was used to determine the mineral abundances and unit-cell parameters of the crystalline minerals in the sample (e.g., Bish & Howard, 1988). Crystalline phases were modeled using a Pearson-VII peak shape function and an amorphous peak was included in the refinements to improve the fit. Scale factors, unit cell parameters, peak width, and shape for each mineral phase were allowed to vary for refinements; however, atomic positions, occupancies, and temperature factors were not refined. No preferred orientation corrections are used as the piezoelectrically shaken sample cell is very effective at randomizing grain orientations.

The abundances of amorphous and poorly ordered components were determined using the program FULLPAT (Chipera & Bish, 2002). FULLPAT operates in a method that is similar to the traditional Reference Intensity

Ratio (RIR) method (e.g., Chung, 1974a) except that it uses entire diffraction patterns instead individual peaks. The method is based on the principle that any observed diffraction pattern is simply the sum of the individual phases that compose the sample. To set up for FULLPAT analyses, a known amount of a corundum ($\alpha\text{-Al}_2\text{O}_3$) internal standard is added to both library standards and unknowns (20wt%) and all individual library patterns are normalized on an equal-corundum basis so that the corundum in each library standard is at the same intensity to facilitate matching the corundum in the library patterns to that in the observed pattern.

Because the amount of corundum added to standards and unknowns is identical, each analysis is reduced to nothing more than scaling and matching of corundum-normalized library patterns to the observed pattern. The analysis is unconstrained and should sum to $\sim 100\%$. However, on Mars, it would be difficult to add an internal standard to a sample. Since all standard phases are normalized to be equal on the basis of the intensity of their corundum internal standard, an “external standard” or “adiabatic” analysis, can be conducted as described by Chung (1974b). Scaling of each library pattern to match the observed pattern yields relative percentages for all phases. The relative percentages are then normalized to sum to 100%.

FULLPAT not only works with samples that contain well-ordered materials but is particularly well suited for samples containing amorphous and/or disordered materials that other methods have difficulty quantifying. As FULLPAT fits entire pattern, including background, multiple amorphous humps, and any other feature, their individual intensity profiles or “amorphous humps” are included in the refinement as they are explicitly considered as individual phases. In many cases, full-pattern fitting may be the best or only method to obtain quantitative results for extremely disordered materials where there is no unique intensity area that can be measured for a traditional (RIR) analysis or where no crystal structure is available for Rietveld refinement (Chiperá & Bish, 2013).

The version of FULLPAT adapted for the MSL mission contains a standard library that has an extensive suite of crystalline minerals, X-ray amorphous and poorly ordered phases (e.g., rhyolitic glass, basaltic glass, palagonite, allophane, ferrihydrite, etc.), along with Kapton (X-ray window material) and linear backgrounds that can all be included in regression. A requirement for FULLPAT is that for each individual phase/material, including the amorphous materials, the XRD pattern has either been measured on a similar XRD instrument or been calculated using the same instrument parameters as the samples being analyzed. Since all patterns are normalized to a reference internal standard intensity, patterns without an added internal standard can still be properly normalized if the RIR is also known or determined (Achilles et al., 2013; Chung, 1974b).

2.3. APXS Data

The Alpha Particle X-ray Spectrometer (APXS) instrument on the MSL rover is capable of determining the chemical composition of rocks and drill-hole fines by combined methods of Particle-Induced X-ray Emission (PIXE) and X-ray fluorescence (XRF) in order to measure major and trace elements from sodium to bromine (Gellert et al., 2006, 2015). APXS uses a spot size of 1.7 cm in diameter when the instrument is close to the sample and averages over all mineral grains in its field of view (Gellert et al., 2015). It should be noted that APXS does not measure the elements lighter than sodium such that H_2O and CO_2 are not included in the analyses. Canaima APXS compositional data were obtained on two brushed spots of the rock surface and on the drill tailings. The tailings measured by the APXS are extracted from a range of depths in the drill hole (Canaima was drilled to a depth of 3.65 cm).

2.4. Water Content Determination Using ChemCam Data

The ChemCam instrument is a laser-induced breakdown spectrometer (LIBS) that provides chemical analyses at a submillimeter scale and detailed images with the Remote Micro Imager (RMI) (Maurice et al., 2016). Water content quantification uses the hydrogen emission peak with a dedicated calibration model (Rapin, Meslin, et al., 2017). Using LIBS for hydrogen quantification requires a surface without significant roughness and cannot be based on a single point analysis; at least 5 are required to assess variability (Rapin, Bousquet, et al., 2017). The target must also be a solid material and target composition in the realm of what has been used in the calibration set. Those requirements are met at the Canaima drill site: laboratory calibration of hydrogen includes Mg and Ca sulfates mixed within a basaltic matrix, and the target is solid bedrock without significant roughness.

2.5. Rover Environmental Monitoring Station (REMS)

The Rover Environmental Monitoring Station (REMS) aboard MSL is comprised of various sensors (Gómez-Elvira et al., 2012), among which the Ground Temperature Sensor (GTS) and the Humidity Sensor (HS) are the focus of

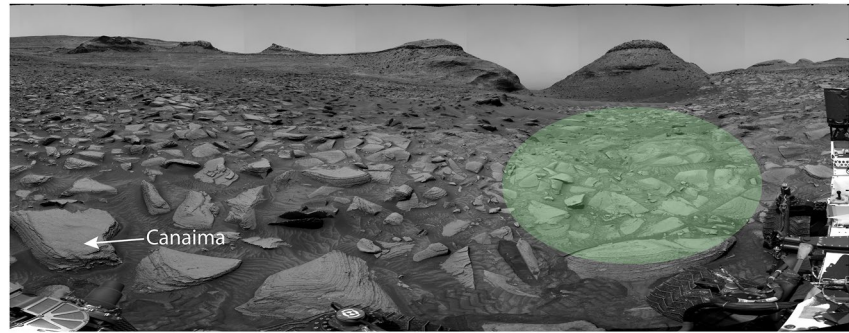


Figure 2. Navcam mosaic with the field of view of the ground temperature sensor during sols 3609–3624 (green shaded region) along with the Canaima drill hole (white arrow). For reference, the distance between Canaima and the center of the green ellipse is ~ 5 m.

this investigation. GTS is a pyrometer measuring the surface brightness temperature (T_g) with a thermopile in the 8–14 μm range (Sebastián et al., 2010). It is located at the base of boom 1 at about 1.6 m above the ground, and it points toward the ground with an azimuth of 120° (with 0° being the rover forward-looking direction, counting clockwise) and an elevation of -26° downward from the plane of the rover deck. This geometry results in a field of view that covers an area of $\sim 100\text{ m}^2$ over flat terrains. As an example, Figure 2 shows the field of view of the GTS on sols 3609–3624, when the rover was parked with an azimuth of 250.34° (W/SW) and a tilt of 0.63° . The HS is mounted on the forward-pointed boom 2 and consists of three polymeric sensors that measure the relative humidity (RH) with respect to ice at 1.6 m above the ground, as well as the temperature of the air entering the HS (T_{RH}) (Harri et al., 2014). REMS nominally measures during the first 5 min of each hour. In addition, 1 hr-long sample periods are interspersed to cover each hour of the sol at least once every six sols (Newman et al., 2017). In both cases, REMS sensors measure at 1 Hz.

The REMS data represent values of measured ground temperature and estimated RH at the ground and GTS and HS measurements were processed as follows. First, the HS measurements are constrained to those of highest confidence, which include only the first few seconds after the HS has been turned on after at least 5 min of inactivity. This was done to avoid spurious effects due to heating (Martínez et al., 2017). These measurements present an uncertainty of 2%, 10%, and 20% for HS temperatures >243 K, between 243 and 203 K, and <203 K, respectively (Martínez et al., 2016). Second, the GTS measurements were considered within a 5'-long interval centered at the time when HS measurements of the highest confidence were taken. The length of this interval was chosen to calculate the averaged values and thus minimize the electric noise present in GTS measurements. This strategy resulted in random uncertainties (1σ) which vary strongly as a function of Local Mean Solar Time (LMST), with maximum values of ~ 6 K during early a.m. hours and minimum values <2 K in the vicinity of noon. Finally, RH is estimated at the ground (RH_g) assuming that the water vapor pressure (e) is constant in the first 1.6 m above the ground. Therefore, $\text{RH}_g \approx e/e_s(\bar{T}_g)$, where $e = \text{RH} \times e_s(T_{RH})$ is the water vapor pressure at 1.6 m obtained directly from HS measurements, e_s is the saturation vapor pressure over ice (Martínez et al., 2016), and \bar{T}_g is the averaged ground temperature.

We note that the estimated nighttime values of RH_g represent an upper bound. The reason is twofold. On one hand, the adsorption of water vapor onto the ground occurs at night (e.g., Savijärvi et al., 2019). Therefore, the water vapor pressure at the ground must be lower than at 1.6 m, which would reduce our estimated values of RH_g (Savijärvi et al., 2019). On another hand, nighttime ground temperature values at the Canaima drill site are likely to be warmer than those measured by the GTS. While Canaima's drill hole was made on bedrock (Figure 2, white arrow), the field of view of the GTS also included fine-grained regolith (Figure 2, green area). Therefore, the thermal inertia of the Canaima bedrock is very likely higher than that of the area sensed by the GTS, which would imply warmer nighttime temperatures and therefore lower RH_g values.

3. Results

3.1. Canaima Drill Hole Mineralogy

For the first time on Mars, one of many possible crystalline Mg-sulfate minerals (Table 1), starkeyite ($\text{MgSO}_4 \cdot 4\text{H}_2\text{O}$), was definitively identified using the CheMin XRD instrument (Figure 3), albeit at low abundance.

Table 1

Listing of Mg-Sulfate Phases Discussed in This Paper

Mineral	Formula
Kieserite	MgSO ₄ ·H ₂ O
Sanderite	MgSO ₄ ·2H ₂ O
Starkeyite	MgSO ₄ ·4H ₂ O
Pentahydrate	MgSO ₄ ·5H ₂ O
Hexahydrate	MgSO ₄ ·6H ₂ O
Epsomite	MgSO ₄ ·7H ₂ O
Meridianiite	MgSO ₄ ·11H ₂ O
Amorphous MgSO ₄	MgSO ₄ ·nH ₂ O (n varies from ~1 to 2)

Canaima is composed mostly of amorphous material (~62 wt%) along with andesine, hematite, goethite, Ca-sulfates (gypsum, bassanite, and anhydrite), pyroxenes, and other minor minerals as crystalline phases (Table 2).

The presence of X-ray amorphous components in the Canaima XRD patterns can be inferred from the appearance of a low-angle rise (<~10° 2θ) and by a broad peak in the background spanning from approximately 15 to 45° 2θ. Figure 4 shows the amorphous components that were refined in the analysis. Rhyolitic glass and amorphous MgSO₄·nH₂O modeled the central “amorphous hump,” although basaltic glass could also be in the pattern as it has a similar pattern to amorphous MgSO₄·nH₂O, but the FULLPAT regressions showed preference for amorphous MgSO₄·nH₂O. The low-2θ angle (<10°) rise is the product of disordered materials such as palagonite, allophane, and ferrihydrite (Achilles et al., 2013). It is likely that several disordered species may be present in the low-2θ angle rise as differences in the patterns used to fit this region are too subtle to distinguish which species; however, the sum of

the components remains unchanged. This disordered material is labeled on Figure 4 as “palagonite-like material” and reported as a single value in Table 2. The Kapton window pattern was from the empty sample cell.

One limitation in the analysis of amorphous materials is that it is not known for certain what the amorphous components are on Mars. FULLPAT may contain library standards whose patterns appear to be similar in shape and features, but similarity in the chemical composition and other properties is unknown. On Mars, due to power requirements, shorter analysis times are used than would be typical on Earth. Consequently, a lower signal to noise ratio is observed in the pattern and it becomes increasingly difficult to distinguish the subtle differences between amorphous species.

3.2. Chemical Composition of the Canaima Sample

3.2.1. Results of APXS Analyses

Amorphous Mg-sulfate (Am-MgSO₄) is believed to be present in the Canaima sample, but its broad XRD diffraction pattern is intermingled with other amorphous phases such that it is difficult to determine from CheMin data alone. To help answer this question, chemical data from the APXS analyses of the brushed Canaima surface and

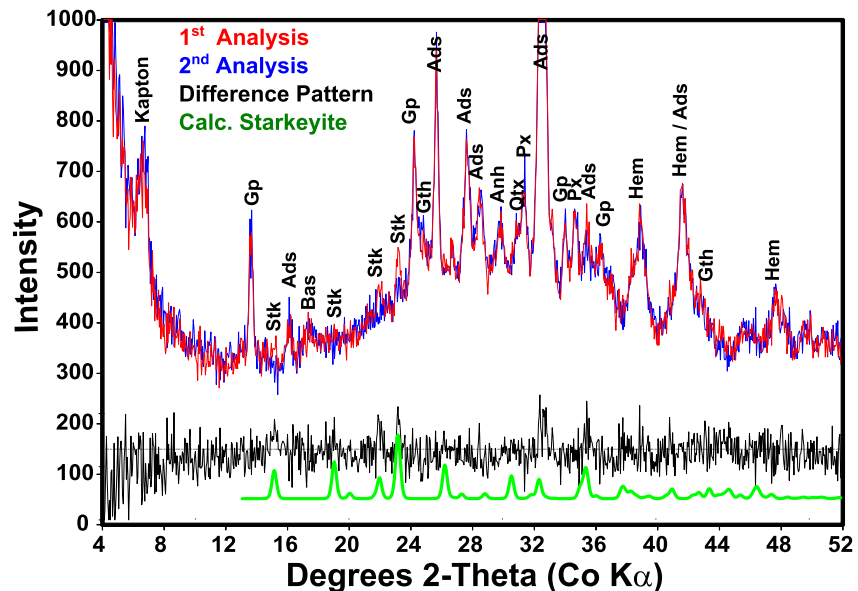


Figure 3. Superimposed patterns of the first (red) and second (blue) overnight analyses. The difference pattern (black) shows the starkeyite that disappeared in the second pattern after it reacted to amorphous MgSO₄·nH₂O while in the rover body. The green pattern is a calculated pattern for starkeyite. Prominent peaks are labeled with the mineral generating the peak as follows: Gp = gypsum; Stk = starkeyite; Ads = andesine; Bas = bassanite; Gth = goethite; Anh = anhydrite; Qtz = quartz; Px = pyroxene; and Hem = hematite.

Table 2
Mineral Abundances (Wt%) for the Three CheMin Analyses of the Canaima Sample

Phase	1st night	3rd night	13th night
Starkeyite	2.3 ± 0.3	0.1 ± 0.2	---
Andesine	16.9 ± 0.6	15.5 ± 0.6	18.0 ± 0.5
Gypsum	4.0 ± 0.2	4.1 ± 0.2	1.5 ± 0.2
Bassanite	0.4 ± 0.3	0.8 ± 0.4	1.7 ± 0.3
Anhydrite	0.6 ± 0.3	1.0 ± 0.4	0.9 ± 0.5
Hematite	4.7 ± 0.4	4.7 ± 0.6	4.8 ± 0.5
Goethite	2.2 ± 0.6	2.2 ± 0.7	2.2 ± 0.6
Quartz	0.5 ± 0.2	0.5 ± 0.3	0.5 ± 0.2
Sanidine	3.2 ± 0.4	2.7 ± 0.6	3.4 ± 0.4
Pyroxene	3.2 ± 1.1	3.4 ± 0.8	3.7 ± 1.1
Amorphous MgSO ₄ ·nH ₂ O	19.4 ± 3.5	20.9 ± 3.5	20.0 ± 3.5
Other Amorphous	29.5 ± 7.4	28.5 ± 7.1	28.7 ± 7.2
Palagonite-Like Material	13.0 ± 3.2	15.6 ± 3.9	14.3 ± 3.6
Total	100.0	100.0	100.0

Note. Errors Represent 1σ Values.

drill tailings were incorporated. The surface and tailings measurements agree well, except for significantly lower Cl and Br concentrations in the tailings derived from deeper inside the rock (Figure 5a). The tailings analysis is most likely to represent the sample delivered to CheMin. Note that APXS analyses of drill fines versus equivalent brushed rock surfaces throughout *Curiosity's* investigation of Gale craters typically show surface enrichment of Cl and Br (top ~0.5 mm) from dust (Berger et al., 2020).

The Canaima analyses revealed elevated total MgO and SO₃ relative to the majority of Mount Sharp group bedrock targets analyzed by APXS (Figure 5a). Figures 5b and 5c show the results of the APXS analyses of rock and drill samples through the transition from the phyllosilicate-rich unit in Glen Torridon into the Mg-sulfate-bearing unit (Figure 1), which includes the Canaima drill site. The majority of targets analyzed from the Mg-sulfate-bearing unit, including Canaima, follow a positive correlation trend between MgO and SO₃, consistent with the addition of up to ~15 wt% Mg-sulfate to typical Mount Sharp bedrock (Figures 5b and 5c). In contrast, the correlation of SO₃ with CaO in the bedrock encountered prior to the “sulfate-bearing unit” is largely consistent with a Ca-sulfate component, with evidence of a ~5–10 wt% Mg-sulfate component mostly associated with diagenetic, nodular targets (Rapin et al., 2021).

3.2.2. Results of ChemCam Analyses

Water abundance using ChemCam for the Canaima sample was measured directly on the surface of Canaima bedrock and along the drill hole wall (Figures 6a and 6b) and was calculated to be 14.2 wt% H₂O (Table 3). Figure 6c shows the 10 ChemCam data points (two 5 × 1 rasters) of 30 shots each acquired with the point-to-point variability in hydrogen relatively low at 20% of the mean value. The low variability is consistent with adequately low surface roughness; therefore, the average hydrogen signal can be used to estimate the bulk water content. The shot-to-shot trend of the hydrogen signal also does not indicate any clear dehydration from the surface inwards within the first hundred microns of the LIBS shot series approximate ablation depth. Instead, it shows a slight decrease in hydrogen with increasing shot number, which may indicate that Mg-sulfate gradually dehydrates due to heating by the repeated laser

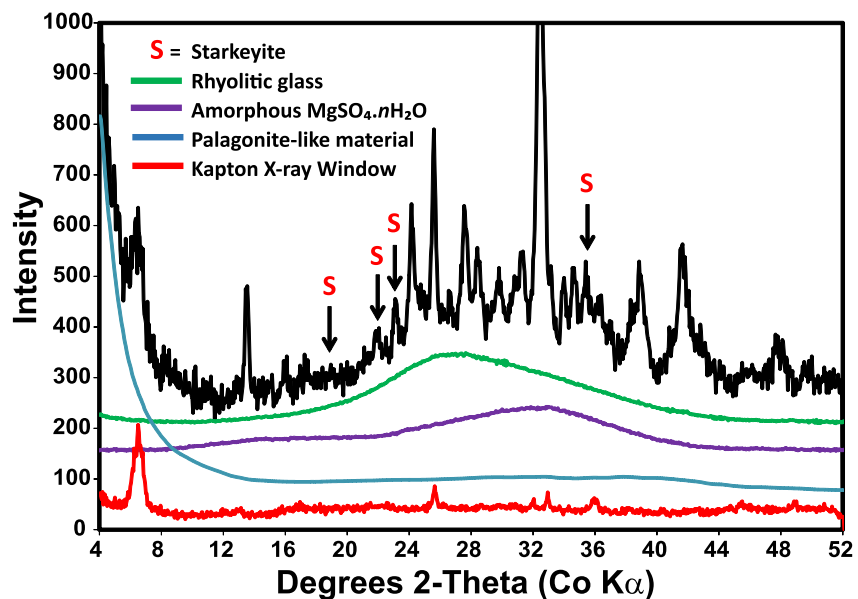


Figure 4. XRD pattern from the first night's analysis at Canaima showing the amorphous components that were refined in the analysis. The Kapton window pattern was from the empty sample cell. The relative intensities (and abundances) for each of the phases are scaled appropriately to the Canaima pattern, but have been offset for better visualization.

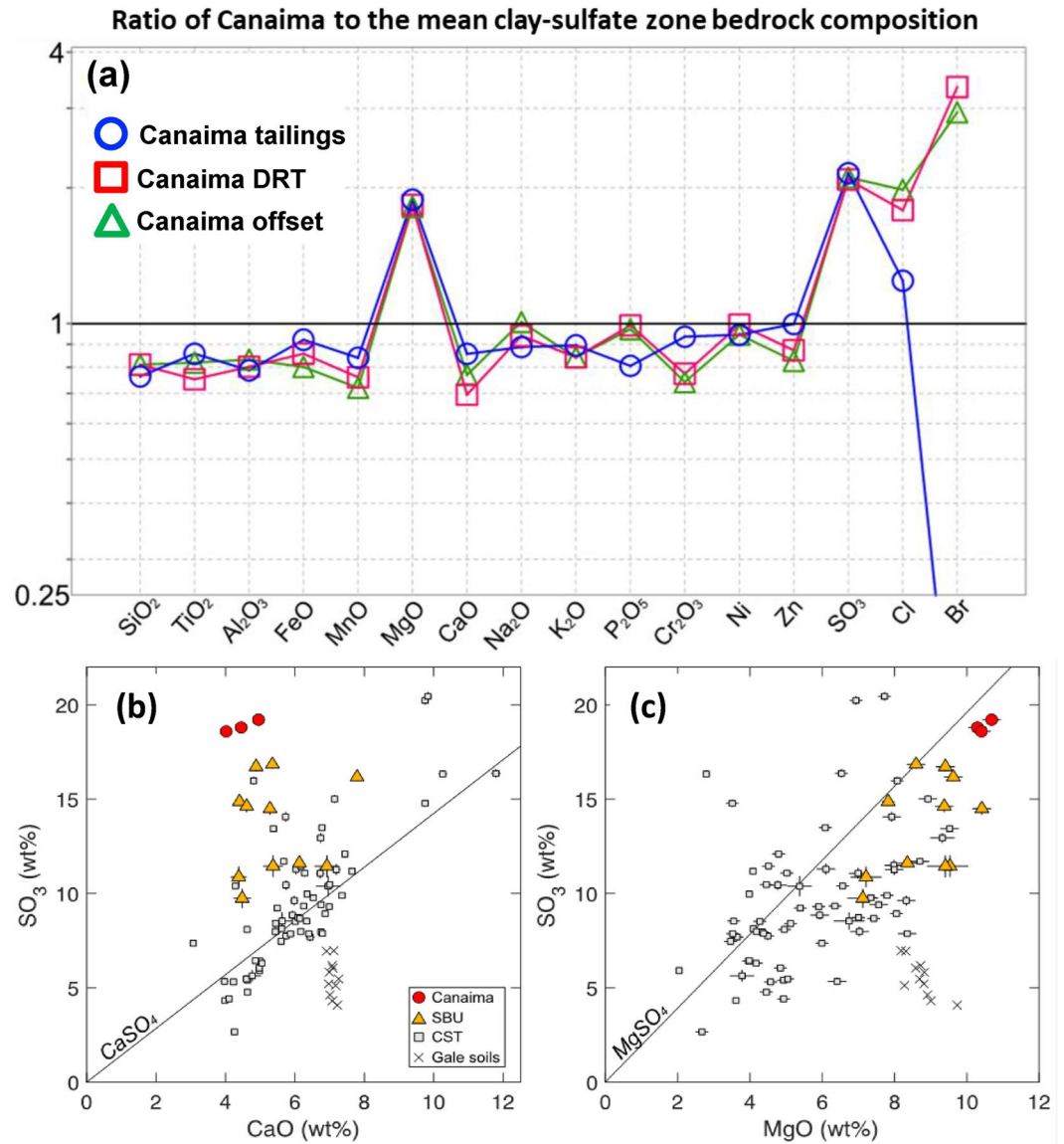


Figure 5. (a) APXS data of Canaima obtained on two brushed surface spots of the rock (Canaima_DRT and Canaima_offset) and on drill tailings (Canaima_tailings). The data are normalized by the mean bedrock of the transitional zone between clay-bearing and sulfate-bearing units. The oxide/element ratios demonstrate that Canaima has roughly the same bulk elemental composition as the stratigraphically underlying bedrock, but with the addition of Mg-sulfate. With the exception of bromine, precision error (Table 3) is contained within the symbols. The Br ratio for the tailings (0.09) is not shown for clarity. APXS results are shown for SO₃ versus (b) CaO and (c) MgO in the transitional zone between clay- and sulfate-bearing units (CST) and in the Mg-sulfate-bearing unit (SBU) where Canaima is located (Figure 1). All APXS targets in the CST (sols 2564 to 3630) are shown with the following omissions: (1) targets with cross-cutting Ca-sulfate veins in the field of view, (2) large 1–3 cm diagenetic nodules, (3) sandstone lenses (Prow/Panari), and (4) five atypically altered targets near an unconformity. Pure CaSO₄ and MgSO₄ lines are shown for reference.

pulses at each point, as also suggested by laboratory experiments using the ChemCam replica (Rapin, Meslin, et al., 2017).

3.3. Calculating Amorphous MgSO₄·nH₂O Composition and Abundance From APXS and ChemCam Data

X-ray amorphous abundances as well as compositions have been estimated from CheMin XRD data using a mass balance calculation (MBC) approach (Smith et al., 2018), which combines the crystalline mineralogy derived

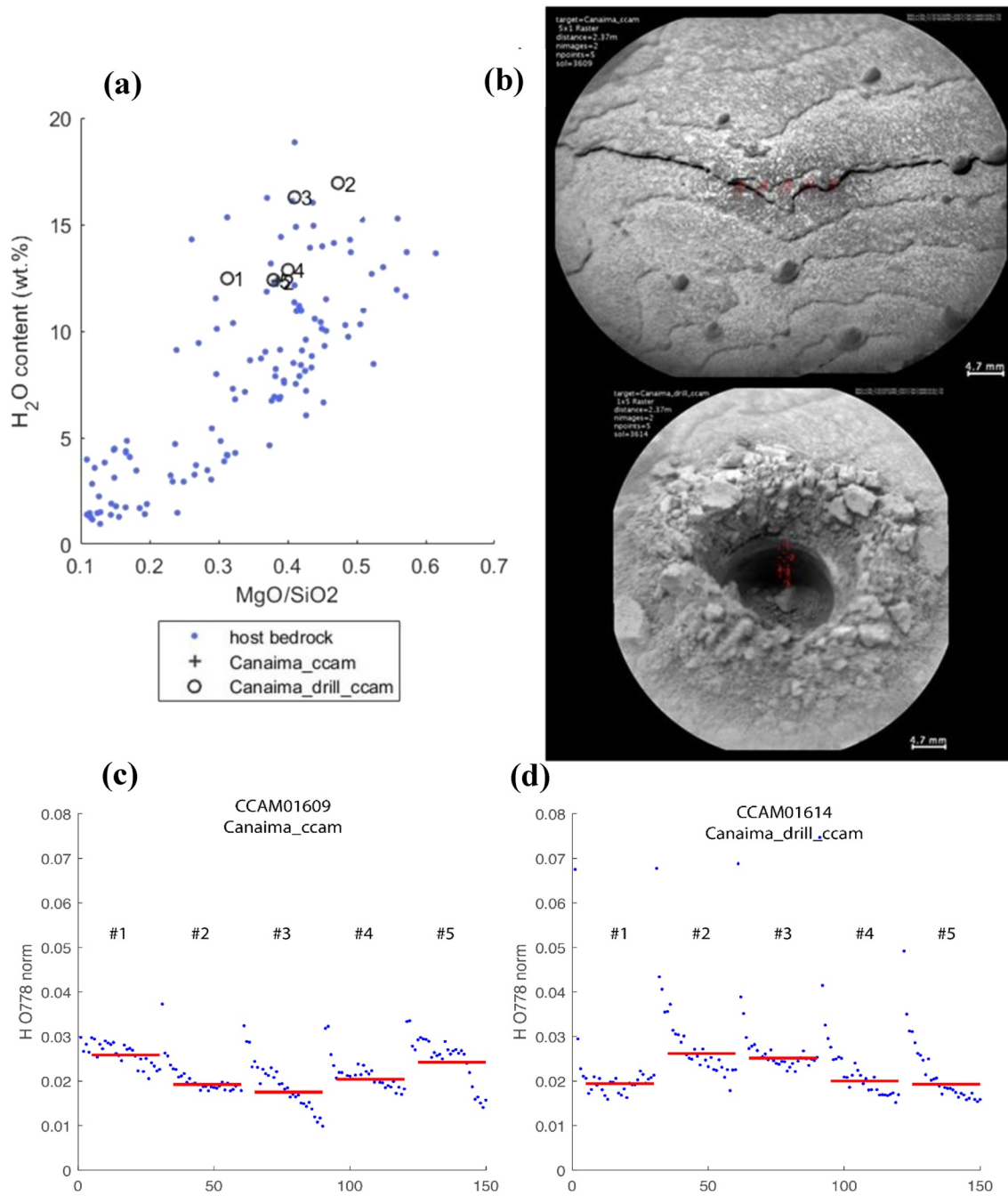


Figure 6. (a) ChemCam data at and near the Canaima drill site showing inferred H₂O content associated with MgO/SiO₂ increase related to the enrichment of Mg-sulfate compared to other bedrock with typical lower hydration. The two 5 × 1 LIBS rasters on Canaima undisturbed surface (Canaima_ccam) and on the drill hole wall (Canaima_drill_ccam) show similar elevated water content averaging at 14.2 wt% H₂O. (b) Context RMI mosaic images for the two rasters with reticles indicating the location of each LIBS analysis is also shown. (c,d) ChemCam shot-to-shot profile of the hydrogen signal (normalized to oxygen at 778 nm as used for estimation of the water content) for the two 5 × 1 rasters (10 points of 30 shots each). Red bars indicate the average hydrogen signal for the shot series at each point after removal of the first 3 shots affected by dust.

from full-pattern fitting analyses of CheMin data using FULLPAT (Chipera & Bish, 2002) with the bulk chemical composition measured by APXS (Gellert et al., 2006, 2015) and water content from ChemCam (Rapin, Meslin, et al., 2017). In this method, the chemical contribution of the crystalline component (calculated from the XRD-derived mineralogy and from unit-cell parameters, Morrison, Downs, Blake, Prabhu, et al., 2018; Morrison, Downs, Blake, Vaniman, et al., 2018) is subtracted from the APXS bulk chemical composition, to provide the

Table 3
Chemical Composition Using APXS Analyses of Canaima Tailings Combined With ChemCam Water Abundances Along With the Calculated Compositions of the Crystalline and Amorphous Fractions

Oxide	Chemical analysis (Wt%) ^a	Crystalline component (Wt%) ^a	Amorphous component (Wt%) ^a
SiO ₂	29.35 ± 0.37	14.1 ± 5.9	15.2 ± 5.7
TiO ₂	0.77 ± 0.03	---	0.77 ± 0.03
Al ₂ O ₃	5.67 ± 0.16	5.3 ± 2.2	0.4 ± 2.1
Cr ₂ O ₃	0.25 ± 0.01	---	0.25 ± 0.01
FeO(T)	15.15 ± 0.17	---	8.7 ± 2.6
FeO	---	0.4 ± 0.4	---
Fe ₂ O ₃	---	6.7 ± 2.9	---
MnO	0.18 ± 0.01	---	0.18 ± 0.01
MgO	9.16 ± 0.21	1.2 ± 0.6	7.9 ± 0.6
CaO	4.25 ± 0.05	3.6 ± 1.5	0.7 ± 1.4
Na ₂ O	1.88 ± 0.12	1.2 ± 0.6	0.7 ± 0.5
K ₂ O	0.58 ± 0.02	0.3 ± 0.3	0.3 ± 0.2
P ₂ O ₅	0.75 ± 0.04	---	0.75 ± 0.04
SO ₃	16.48 ± 0.19	3.4 ± 1.4	13.0 ± 1.5
Cl	1.09 ± 0.03	---	1.09 ± 0.03
H ₂ O	14.20 ± 2.3	2.0 ± 0.8	12.1 ± 2.4
Ni (ppm)	839 (45)		
Zn (ppm)	1025 (35)		
Br (ppm)	22 (5)		

^aPrecision Errors are 1σ Values.

composition of the amorphous component. Since this method relies on careful analysis of the crystalline components, any errors in the fitting will propagate into the MBC estimates. Results for the Canaima sample are shown in Table 3.

The amorphous fraction shows high concentrations of SiO₂, FeO, MgO, and SO₃. It is difficult to say in which of the possible amorphous phases the residual components exist. The SiO₂ seen in the amorphous fraction is likely to be in a volcanic or impact-produced glass or a palagonite-like amorphous material. The FeO could be in glass, sulfate, palagonitic-material, or most likely ferrihydrite. However, the elevated MgO and SO₃ strongly suggest an amorphous MgSO₄·nH₂O phase is present. By combining the MgO and SO₃ until one of them is consumed, maximum abundance of ~28 wt% MgSO₄ is calculated with SO₃ consumed first leaving excess MgO. The occurrence of Am-MgSO₄ at Canaima is in line with the observations of Smith et al., 2022 who note strong evidence for SO₃ in the amorphous fraction for rocks and soils along *Curiosity's* path, although at much lower abundance with Mg, Fe, and Ca varieties all possible.

It is important to note a few limitations of the MBC method. First, the composition of crystalline phases that were not identified or are below the detection limit of XRD will be allocated to the amorphous component composition. Second, crystalline minerals frequently contain minor elemental substitutions not reported in their ideal structure formula. Lastly, the sample analyzed by CheMin and the drill tailings analyzed by APXS are not the same sample so any variability seen in the drill hole mineralogy could affect the relative compositions of the two samples. Nevertheless, prior work has shown the utility of this approach (e.g., Bristow et al., 2021; Morrison, Downs, Blake, Vaniman, et al., 2018; Rampe et al., 2020; Thorpe et al., 2022).

Water abundance calculated using ChemCam data was 14.2 wt% H₂O for the sample and subtracting from it the water abundances calculated from the mineralogy of the crystalline fraction provides the water content of the

amorphous fraction. To calculate the upper possible water content of the amorphous-sulfate phase, the water content for the “palagonite-like material” must also be subtracted. It is uncertain as to the exact mineralogy of the “palagonite-like material”, but the assumption is made that it is all palagonite (or a similar phase and water content). Milliken and Mustard (2005) measured the water content in their palagonite sample at 17.9 wt% water. Using 17.9 wt% water for palagonite, the amorphous sulfate phase in Canaima was calculated to have a water content of 3.2 mol per amorphous-SO₄ formula unit.

3.4. Starkeyite Stability and Implications for Climate Changes

3.4.1. Environmental Conditions for the Canaima Drill Sample

Three overnight analyses were conducted on the Canaima sample over 13 sols. The first night's analysis began just after the end of sol 3614 about 9 hours after the sample was delivered to CheMin (Figure 7). Measured ground temperature and estimated ground relative humidity (RH) at the Canaima site varied from ~ -70°C to 1°C and ~65%~0.5% for nighttime to daytime, respectively, during the time interval between sample acquisition through data analysis (Figure 8). The temperature cycle inside the rover body varied from ~6 to 30°C, which implies extremely low RH (<<0.1%) during the day. Starkeyite was unambiguously identified in the first night's analysis, albeit at a low abundance (Table 2). A second analysis took place two nights later (end of sol 3616) after the sample experienced two diurnal cycles inside the rover body. Starkeyite, if still present, was below CheMin's detection limit (<~0.3 wt%) and no other Mg-sulfate minerals were detected indicating that Am-MgSO₄ was produced, consistent with experimental data showing that polyhydrated crystalline Mg-sulfates become amorphous at very low RH (Chipera & Vaniman, 2007; Vaniman & Chipera, 2006; Vaniman et al., 2004, 2007; Wang et al., 2007, 2009). The third analysis took place 11 nights (and thermal cycles) later (end of sol 3627), and, again,

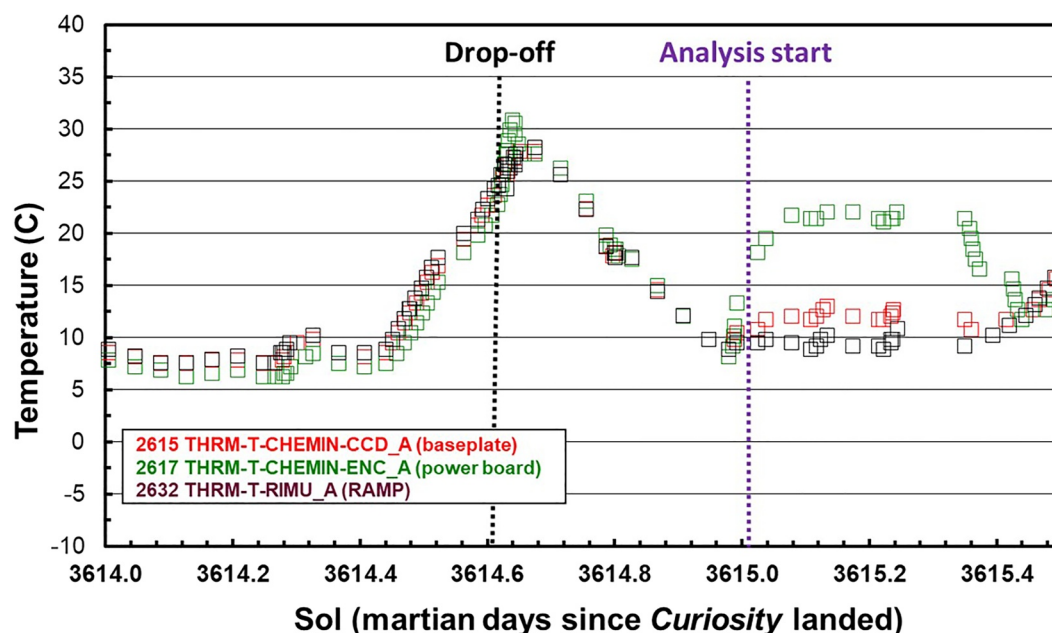


Figure 7. Temperatures measured inside the *Curiosity* Rover during the delivery of the Canaima sample to CheMin, and at the start of the first night's analysis. Temperatures were recorded at the baseplate for the CheMin CCD detector, at the CheMin ENC power board, and on the Rover Avionics Mounting Plate (RAMP), which is the interface to which the CheMin instrument is bolted.

no crystalline Mg-sulfates (including starkeyite) were observed. Ca-sulfates have been shown to dehydrate over time inside the CheMin instrument (Vaniman et al., 2018) and this was also observed for the Canaima sample with gypsum starting to dehydrate to bassanite between the second and third analysis.

As noted above, conditions inside the rover show higher temperatures and extremely low RH compared to surface conditions. The Canaima drill sample was delivered into CheMin during the day just before the peak internal temperature ($\sim 28^{\circ}\text{C}$), where it remained for ~ 9 hours as it cooled to nighttime temperature before the first analysis commenced (Figure 7). As it went through one half of a diurnal temperature cycle before the first analysis was conducted, it is likely that some starkeyite altered to Am-MgSO₄ and the original starkeyite abundance in Canaima is higher than we reported for the first analysis (Table 2). This is corroborated by the bulk hydration measured using ChemCam at 14.2 wt% H₂O (Table 3), indicating that the amorphous-sulfate phase in Canaima has a maximum water content of 2.8–3.4 waters per amorphous-SO₄ unit (a hydration level closer to starkeyite, Table 1) depending on the amount of water attributed to the palagonite-like material in the sample. The environmental conditions observed at Canaima and the observed transformation of starkeyite to Am-MgSO₄ within the rover body suggest that returning samples to Earth without subsequent alteration of the Mg-sulfate mineralogy would be extremely difficult.

3.4.2. Stability Relations Between Mg-Sulfate Phases

Mg-sulfates are extremely sensitive to temperature and RH conditions and will recrystallize and exchange water with the environment to form different hydrates in response to changing environmental conditions. The stabilities of Mg-sulfate minerals, specifically with application to Mars, have been studied extensively in laboratory experiments (e.g., Chipera & Vaniman, 2007; Vaniman & Chipera, 2006; Vaniman et al., 2004, 2007; Wang et al., 2007, 2009, 2011). Figure 8 shows a summary of experimental work superimposed on stability fields for Mg-sulfates stylized after Grevel and Dachs, 2012 who conducted thermodynamic calculations and compiled literature data (Chou & Seal, 2003, 2007; Lallemand et al., 1974; Steiger et al., 2011), along with the approximate phase boundaries determined from experimental data (Chipera & Vaniman, 2007; Vaniman & Chipera, 2006; Vaniman et al., 2007; Wang et al., 2009, 2011). Figure 8 can be used to predict which Mg-sulfate species are thermochemically stable with changes in martian climate; however, chemical reactions among the Mg-sulfates are known to be kinetically inhibited at Mars surface temperatures, to be path dependent, and to exhibit broad ranges of metastability (Chipera & Vaniman, 2007; Vaniman & Chipera, 2006; Vaniman et al., 2007; Wang

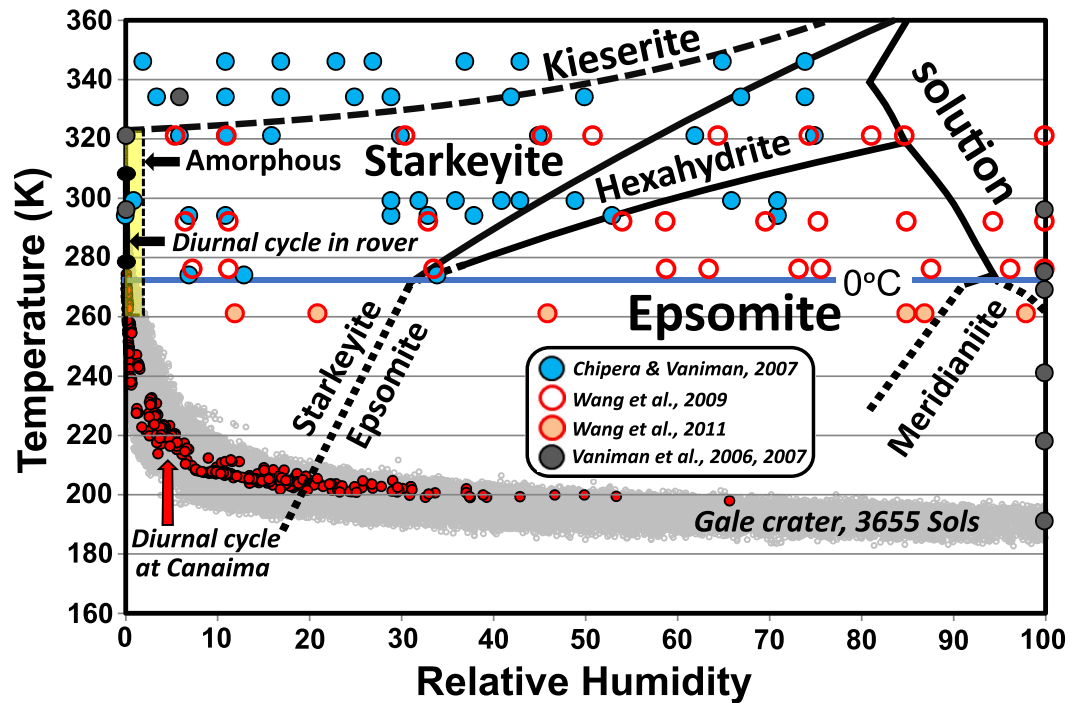


Figure 8. Stability fields in the Mg-sulfate system stylized after (Grevel & Dachs, 2012) along with approximate phase boundaries determined from the experimental data (Chipera & Vaniman, 2007; Wang et al., 2011) and approximate region where Am-MgSO₄ forms (Yellow box, Vaniman et al., 2007). Plotted are the T-RH locations of published experimental data (Chipera & Vaniman, 2007; Vaniman & Chipera, 2006; Vaniman et al., 2007; Wang et al., 2009, 2011), the seasonal Gale crater ground temperatures and estimated ground RH (gray circles), the diurnal cycle ground temperatures and estimated ground RH at Canaima during sols 3609–3625 (red filled circles), the diurnal cycle ground temperatures and estimated ground RH in the rover body (between the two black dots at 0% RH in the middle of the amorphous MgSO₄·nH₂O field). It should be noted that estimated RH are maximum values and real values can be much lower.

et al., 2009). To constrain the environmental conditions in Gale crater, Figure 8 shows the measured ground temperatures and estimated ground RH at the beginning of the mission (gray circles, first 3655 sols) (e.g., Martinez et al., 2017, 2021) and the summer daily diurnal conditions (filled red circles, sols 3609–3625) by the Canaima drill hole (Figure 2), and inside of the rover.

It should be noted that estimated nighttime values of RH at the ground represent an upper bound based on the method used to derive them. Figure 8 shows that starkeyite and Am-MgSO₄ are the phases expected to be present for summer-like conditions in Gale crater. The presence of starkeyite is significant because it rarely occurs on Earth and demonstrates the unique climate conditions on Mars. Several studies suggest that starkeyite is metastable (Chou & Seal, 2007; Grevel & Dachs, 2012; Steiger et al., 2011). However, it occurs in Gale crater and is shown to be a stable reaction product covering a large section of T–RH space in experimental studies of Mg-sulfate stability (e.g., Chipera & Vaniman, 2007; Wang et al., 2009, 2011).

There are few experimental data on Mg-sulfate that represent the winter conditions encountered in Gale crater as it is difficult to control RH at temperatures below 0°C and reaction rates decrease significantly as temperature decreases. Wang et al., 2011 conducted experiments at –10°C and <20% RH. Starting with epsomite, starkeyite, and kieserite, even though not in their thermodynamic stability region (Figure 8), no reaction occurred to another Mg-sulfate during laboratory timescales of ~3.8 years demonstrating the sluggishness of these reactions at low temperatures. The Mg-sulfate stability fields shown in Figure 8 suggest that the reaction back and forth between starkeyite and epsomite, with their differing hydration states, could play a dominant role in the daily water cycle of Mars away from the polar ice caps as suggested by Chou & Seal, 2007. However, this is not supported by the observed kinetics where dehydration at Mars summer day-time temperatures readily forms starkeyite and Am-MgSO₄, but at lower night-time temperatures, are too sluggish to revert back to epsomite. Experimental data using water ice to control RH at 100% and at Mars winter temperature (193K) show that Am-MgSO₄ is extremely resistant to rehydration with no reaction evident after ~2,000 days (Vaniman & Chipera, 2006; Vaniman

et al., 2007). The implication of this is that once highly hydrated Mg-sulfates (e.g., epsomite $\text{MgSO}_4 \cdot 7\text{H}_2\text{O}$, or meridianiite $\text{MgSO}_4 \cdot 11\text{H}_2\text{O}$) become dehydrated to starkeyite or Am- MgSO_4 during martian summers, rehydration would not happen over a martian winter. Thus, starkeyite and Am- MgSO_4 are likely to be the dominant Mg-sulfates in Gale crater throughout the entire martian year. It is important to note that even though daily and annual cycles may be too short for hydration-recrystallization, longer duration obliquity cycles on Mars can deliver water ice to lower latitudes where it may persist for much longer periods and promote crystallization of higher hydrates (Vaniman et al., 2007).

4. Discussion

4.1. Mg-Sulfates in Relation to Mars Climate/History

Mg-sulfate minerals have been predicted to occur on the surface of Mars since the first Viking landings in 1976 showed elevated sulfur abundances in the regolith (Clark et al., 1976) and have subsequently been mapped in many locations from orbit. For example, visible/near-infrared spectra collected by the Observatoire pour la Minéralogie, l'Eau, les Glaces et l'Activité (OMEGA) on the Mars Express orbiter show evidence for kieserite ($\text{MgSO}_4 \cdot \text{H}_2\text{O}$) and a broad spectral class of “polyhydrated Mg-sulfates” in several layered terrains across Mars (e.g., Gendrin et al., 2005), although the exact species of these polyhydrated Mg-sulfates were speculative. At the Canaima drill site, CheMin measurements have definitively identified the polyhydrated Mg-sulfates at this location as starkeyite and Am- MgSO_4 . Any kieserite at Gale crater is unlikely to be forming today based on the current seasonal temperature - RH conditions (Figure 8). Its presence seen in a more recent drill sample ~27 m stratigraphically above Canaima (Tapo Caparo), to be discussed in a future paper, presents an enigma as it requires temperatures above 50°C to form from polyhydrated Mg-sulfates (Chipera & Vaniman, 2007; Wang et al., 2009) which are reached only in limited localities on Earth's surface. Further studies of the Mg-sulfates in upper Mount Sharp are in progress and will be supplemented as *Curiosity* progresses to higher strata.

Canaima has the most Mg-sulfate yet seen at Gale crater, but there is evidence of Mg-sulfate in deeper sediments in lesser amounts. Rapin et al. (2019) describe a horizon of hydrated Mg-sulfate 410 m below Canaima. This is in an interval of high salinity, with desiccation cracks that suggest an evaporite origin. Unfortunately, this interval was crossed during an extended period when the sampling system on MSL was not functioning, so there are no XRD data. Rampe et al. (2020) describe Mg,Ni-sulfate concretions in the Pahrump Hills, 580 m below Canaima, where CheMin data show an association with jarosite. Rampe et al. relate these concretions (likely amorphous) to Ni mobilization by mildly acidic groundwater.

Mg-sulfates on Mars were likely derived from sulfate-laden brines evaporating at the surface to precipitate epsomite at temperatures above 2°C or meridianiite below 2°C (Peterson & Wang, 2006), or from freezing brine precipitating meridianiite (e.g., Genceli et al., 2009; Toner et al., 2014). As Mars dried out with changing climate, the epsomite and/or meridianiite that had precipitated would have recrystallized to less-hydrated Mg-sulfate phases following a possible sequence in the order of meridianiite (11 hydrate) > epsomite (7 hydrate) > hexahydrite (6 hydrate) > starkeyite (4 hydrate) > then to either Am- MgSO_4 or to kieserite depending on climate conditions (Chipera & Vaniman, 2007; Wang et al., 2009). Rehydration reactions at elevated RH show that starkeyite and Am- MgSO_4 transform to hexahydrite or epsomite (Figure 8). Kieserite, however, is extremely persistent and will rehydrate only to hexahydrite or epsomite bypassing both starkeyite and Am- MgSO_4 (Chipera & Vaniman, 2007; Grevel & Dachs, 2012; Wang et al., 2009, 2011). Thus, the occurrence of starkeyite at Canaima serves as a climate indicator as it is inferred to be a dehydration product from epsomite or meridianiite in response to a drier climate and environmental conditions were not attained to form kieserite.

The high abundance of Mg-sulfate at Canaima (~22 wt%) is significant. To obtain such abundances, and the thick sequences of sulfate inferred to be present around Mt Sharp (Sheppard et al., 2021), significant volumes of water would have to have been evaporated or sublimated—achieving epsomite saturation from dilute Mars waters requires 100 to 1,000× evapoconcentration (Tosca et al., 2005). On Earth, epsomite is typically present in playas, alkali-salt soil efflorescences, or as efflorescences on stone building materials and monuments (e.g., Kramer et al., 2011). Seasonal or intermittent events, such as rainfall, will dissolve and remove much of these salts, thus requiring re-accumulation of brines to again precipitate salts. With progressively drier Mars conditions, there were fewer re-wetting events which would allow the salts to accumulate without subsequent liquid water removal. The presence of highly soluble Mg-sulfates (starkeyite and Am- MgSO_4) at Canaima suggests negligible aqueous fluid flow through the bedrock post-Mg-sulfate deposition.

Marion et al. (2009) propose two possible mechanisms for the formation of Mg-sulfate in the Burns formation of the Meridiani Planum region of Mars. (a): Brines reached the surface and precipitated salts as efflorescence through saline groundwater evaporation or (b): Playa lake evaporation with eolian contributions (Marion et al., 2009). Similar mechanisms may be proposed for Gale crater. Mineral precipitation from evaporating brines is a function of solubility and ion concentrations in the brine solutions and generally results in numerous co-precipitated mineral phases. In a simple depositional model, Ca-sulfates have lower solubility and would have precipitated earlier in the evolution of the brine lower in the stratigraphic column if sulfates precipitated from upwelling groundwater. Ca-sulfates (gypsum, bassanite, anhydrite), separately or together, have been almost ubiquitous in every drill hole in Gale crater to date (Vaniman et al., 2018). Mg-sulfates have a higher solubility product and would remain in solution until the higher concentration required to saturate the brine was attained to allow them to precipitate.

A hybrid mechanism can be proposed for martian sulfate deposits as Mars is an environment significantly different from Earth. On Earth, sulfates that form in efflorescence and playa lake deposits will dissolve and remobilize due to reoccurring precipitation events. A later-stage drier Mars would not have these precipitation events and it is likely that once brines do reach the surface and precipitate, regardless of the mechanism, the main weathering events will be erosion from wind and particle abrasion. Sulfate minerals found in the Aeolian deposits represented by Canaima could have been redeposited as detritus and dust in eolian sediments with no evidence of their original (chemical precipitation) deposition remaining. Alternatively, re-wetting events under a drier and colder Mars could have resulted in the remobilization of sulfates during seasonal or obliquity-driven freeze-thaw cycles, causing the movement of sulfates in the subsurface.

From evaporating or freezing brine, Mg-sulfates would show up higher in the stratigraphic column or to the center of an evaporite deposit with meridianiite forming at temperatures below 2°C and epsomite at temperatures above 2°C. However, orbital reflectance observations show evidence for kieserite in areas across the martian surface, including Gale crater (e.g., Sheppard et al., 2021), and kieserite has been detected stratigraphically by CheMin above Canaima at the Tapo Caparo drill site. Elevated temperatures are required for kieserite to form. It will precipitate from the brine solution if temperatures are >69° (Chou & Seal, 2003; Grevel & Dachs, 2012) or as a dehydration product of polyhydrated Mg-sulfates at temperatures >50° (Chipera & Vaniman, 2007; Wang et al., 2009, 2011)—see Figure 8. To get the elevated temperatures, some source of heat would be required. For example, it has been proposed by Rodriguez & Van Bergen, 2016 and references therein that hydrothermal systems could deliver heat and water, generate sulfuric acid resulting in the dissolution of rock, and precipitate thick sequences of sulfates as the fluids exit to the surface.

Another mechanism that may be more plausible at Gale crater and elsewhere on Mars is solar-heating of the surface. Kong et al. (2014) propose that sunlight on the surface along with the wind may have facilitated the dehydration process to form kieserite from hexahydrate that they identify at the Dalangtan Playa, China. Kieserite was observed on the very surface of the deposits with progressively more hydrated Mg-sulfates, sanderite (2W; W = hydration number; 2W = 2-hydrate, etc.) starkeyite (4W), pentahydrate (5W), and finally hexahydrate (6W) all occurring within only a cm or two of the surface and suggest that the widespread kieserite on Mars may have formed under similar conditions.

Although the discovery of starkeyite in Gale crater will significantly help interpret Mars climate and processes, a more complete understanding of the paragenesis of Mg-sulfate minerals in Gale crater will have to await *Curiosity's* further analysis of sulfate-rich units at higher elevations on Mount Sharp.

Data Availability Statement

All *Curiosity* data presented in this paper are archived in the NASA Astrobiology and Habitable Environments Database and can be accessed using (Bristow & Chipera, 2023). Additional APXS data can be found in Gellert (2013).

References

- Achilles, C. N., Morris, R. V., Chipera, S. J., Ming, D. W., & Rampe, E. B. (2013). X-ray diffraction reference intensity ratios of amorphous and poorly crystalline phases: Implications for CheMin on the Mars Science Laboratory Mission. *Lunar and Planetary Science Conference, XLIV*. Abstract 3072.
- Berger, J. A., Gellert, R., Boyd, N. I., King, P. L., McCraig, M. A., O'Connell-Cooper, C. D., et al. (2020). Elemental composition and chemical evolution of geologic materials in Gale crater, Mars: APXS results from Bradbury landing to the Vera Rubin ridge. *Journal of Geophysical Research: Planets*, 125(12), e2020JE006536. <https://doi.org/10.1029/2020JE006536>

Acknowledgments

We thank M. Velbel, R. Peterson, and 2 anonymous reviewers for helping improve the manuscript. We acknowledge the support of the Jet Propulsion Lab engineering and management teams and MSL science team members who participated in tactical and strategic operations, without whom the data presented here could not have been collected. Some of this research was carried out at the Jet Propulsion Laboratory, California Institute of Technology, under a contract with the National Aeronautics and Space Administration (NASA). Some co-authors acknowledged funding from the MSL Participating Scientist Program. The MSL APXS instrument and operations were supported by the Canadian Space Agency contract 9F52-19-0632. E.F work was carried out under a contract with the National Aeronautics and Space Administration (NASA) contract 1449038.

- Bish, D. L., & Howard, S. A. (1988). Quantitative phase analysis using the Rietveld method. *Journal of Applied Crystallography*, 21(2), 86–91. <https://doi.org/10.1107/S0021889887009415>
- Blake, D., Vaniman, D., Achilles, C., Anderson, R., Bish, D., Bristow, T., et al. (2012). Characterization and calibration of the CheMin mineralogical instrument on Mars science laboratory. *Space Science Reviews*, 170(1–4), 341–399. <https://doi.org/10.1007/s11214-012-9905-1>
- Bristow, T., & Chipera, S. (2023). Data from: Mineralogical investigation of Mg-sulfate at Gale crater, Mars. Astrobiology Habitable Environment Database. <https://doi.org/10.48667/4apc-vz90>
- Bristow, T. F., Grotzinger, J. P., Rampe, E. B., Cuadros, J., Chipera, S. J., Downs, G. W., et al. (2021). Brine-driven destruction of clay minerals in Gale crater, Mars. *Science*, 373(6551), 198–204. <https://doi.org/10.1126/science.abg5449>
- Chipera, S. J., & Bish, D. L. (2002). FULLPAT: A full-pattern quantitative analysis program for X-ray powder diffraction using measured and calculated patterns. *Journal of Applied Crystallography*, 35(6), 744–749. <https://doi.org/10.1107/S0021889802017405>
- Chipera, S. J., & Bish, D. L. (2013). Fitting full X-ray diffraction patterns for quantitative analysis: A method for readily quantifying crystalline and disordered phases. *Advances in Materials Physics and Chemistry*, 03(01), 47–53. <https://doi.org/10.4236/ampc.2013.31.A007>
- Chipera, S. J., & Vaniman, D. T. (2007). Experimental stability of magnesium sulfate hydrates that may be present on Mars. *Geochimica et Cosmochimica Acta*, 71(1), 241–250. <https://doi.org/10.1016/j.gca.2006.07.044>
- Chou, I.-M., & Seal, R. R., II. (2003). Determination of epsomite-hexahydrite equilibria by the humidity-buffer technique at 0.1 MPa with implications for phase equilibria in the system MgSO₄-H₂O. *Astrobiology*, 3, 619–630. <https://doi.org/10.1089/153110703322610708>
- Chou, I.-M., & Seal, R. R., II. (2007). Magnesium and calcium sulfate stabilities and the water budget of Mars. *Journal of Geophysical Research*, 112(E11), E11004. <https://doi.org/10.1029/2007JE002898>
- Chung, F. H. (1974a). Quantitative interpretation of X-ray diffraction patterns of mixtures. I. Matrix-flushing method for quantitative multicomponent analysis. *Journal of Applied Crystallography*, 7(6), 519–525. <https://doi.org/10.1107/S0021889874010375>
- Chung, F. H. (1974b). Quantitative interpretation of X-ray diffraction patterns of mixtures. II. Adiabatic principle of X-ray diffraction analysis of mixtures. *Journal of Applied Crystallography*, 7(6), 526–531. <https://doi.org/10.1107/S0021889874010387>
- Clark, B. C., Baird, A. K., Rose, H. J., Jr., Toulmin, P., III., Keil, K., Castro, A. J., et al. (1976). Inorganic analyses of martian surface samples at the Viking landing sites. *Science*, 194(4271), 1283–1288. <https://doi.org/10.1126/science.194.4271.1283>
- Fraeman, A. A., Arvidson, R. E., Catalano, J. G., Grotzinger, J. P., Morris, R. V., Murchie, S. L., et al. (2013). A hematite-bearing layer in Gale crater, Mars: Mapping and implications for past aqueous conditions. *Geology*, 41(10), 1103–1106. <https://doi.org/10.1130/G34613.1>
- Fryberger, S. G., & Schenk, C. J. (1988). Pin stripe lamination—A distinctive feature of modern and ancient eolian sediments. *Sedimentary Geology*, 55(1–2), 1–15. [https://doi.org/10.1016/0037-0738\(88\)90087-5](https://doi.org/10.1016/0037-0738(88)90087-5)
- Gellert, R. (2013). MSL Mars alpha particle X-ray spectrometer 4/5 RDR V1.0. NASA Planetary Data System. <https://doi.org/10.17189/1518757>
- Gellert, R., Clark, B. C., III., & MER Science Teams (2015). In situ compositional measurements of rocks and soils with the alpha particle X-ray spectrometer on NASA's Mars rovers. *Elements*, 11(1), 39–44. <https://doi.org/10.2113/gselements.11.1.39>
- Gellert, R., Rieder, R., Brückner, J., Clark, B. C., Dreibus, G., Klingelhöfer, G., et al. (2006). Alpha particle X-ray spectrometer (APXS): Results from Gusev crater and calibration report. *Journal of Geophysical Research*, 111(E2), E02S05. <https://doi.org/10.1029/2005JE002555>
- Genceli, F. E., Horikawa, S., Iizuka, Y., Sakurai, T., Hondoh, T., Kawamura, T., & Witkamp, G.-J. (2009). Meridianiite detected in ice. *Journal of Glaciology*, 55(189), 117–122. <https://doi.org/10.3189/002214309788608921>
- Gendrin, A., Mangold, N., Bibring, J.-P., Langevin, Y., Gondet, B., Poulet, F., et al. (2005). Sulfates in martian layered terrains: The OMEGA/Mars Express view. *Science*, 307(5715), 1587–1591. <https://doi.org/10.1126/science.1109087>
- Gómez-Elvira, J., Armiens, C., Castañer, L., Domínguez, M., Genzer, M., Gómez, F., et al. (2012). REMS: The environmental sensor suite for the Mars Science Laboratory rover. *Space Science Reviews*, 170(1–4), 583–640. <https://doi.org/10.1007/s11214-012-9921-1>
- Grevel, K.-D., Dachs, E., Benisek, A., Steiger, M., Fortes, A. D., & Marler, B. (2012). Experimentally determined standard thermodynamic properties of synthetic MgSO₄·4H₂O (starkeyite) and MgSO₄·3H₂O: A revised internally consistent thermodynamic data set for magnesium sulfate hydrates. *Astrobiology*, 12(11), 1042–1054. <https://doi.org/10.1089/ast.2012.0823>
- Harri, A.-M., Genzer, M., Kempainen, O., Gomez-Elvira, J., Haberle, R., Polkko, J., et al. (2014). Mars Science Laboratory relative humidity observations: Initial results. *Journal of Geophysical Research: Planets*, 119(9), 2132–2147. <https://doi.org/10.1002/2013JE004514>
- Kong, W. G., Zheng, M. P., Kong, F. J., & Chen, W. X. (2014). Sulfate-bearing deposits at Dalangtan Playa and their implication for the formation and preservation of martian salts. *American Mineralogist*, 99(2–3), 283–290. <https://doi.org/10.2138/am.2014.4594>
- Kramer, S., Mirtič, B., Knöller, K., & Rogan-Šmuc, N. (2011). Weathering of the black limestone of historical monuments (Ljubljana, Slovenia): Oxygen and sulfur isotope composition of sulfate salts. *Applied Geochemistry*, 26(9–10), 1632–1638. <https://doi.org/10.1016/j.apgeochem.2011.04.02>
- Lallemant, M., Watelle, G., Boinon, B., Rievière, M., & Cohen-Addad, R. (1974). Contribution à l'étude du système binaire MgSO₄-H₂O: tensions de vapeur des solutions saturées et tensions de dissociation des hydrates successifs. *Revue de Chimie Minerale*, 11, 113–122.
- Marion, G. M., Catling, D. C., & Kargel, J. S. (2009). Br/Cl partitioning in chloride minerals in the Burns formation on Mars. *Icarus*, 200(2), 436–445. <https://doi.org/10.1016/j.icarus.2008.12.004>
- Martínez, G. M., Fischer, E., Rennó, N. O., Sebastián, E., Kempainen, O., Bridges, N., et al. (2016). Likely frost events at Gale crater: Analysis from MSL/REMS measurements. *Icarus*, 280, 93–102. <https://doi.org/10.1016/j.icarus.2015.12.004>
- Martínez, G. M., Newman, C. N., De Vincente-Retortillo, A., Fischer, E., Renno, N. O., Richardson, M. I., et al. (2017). The modern near-surface martian climate: A review of in-situ meteorological data from Viking to Curiosity. *Space Science Reviews*, 212(1–2), 295–338. <https://doi.org/10.1007/s11214-017-0360-x>
- Martínez, G. M., Vicente-Retortillo, A., Vasavada, A. R., Newman, C. E., Fischer, E., Rennó, N. O., et al. (2021). The surface energy budget at Gale crater during the first 2500 sols of the Mars Science Laboratory mission. *Journal of Geophysical Research: Planets*, 126(9), e2020JE006804. <https://doi.org/10.1029/2020JE006804>
- Maurice, S., Clegg, S. M., Wiens, R. C., Gasnault, O., Rapin, W., Forni, O., et al. (2016). ChemCam activities and discoveries during the nominal mission of the Mars science laboratory in Gale crater, Mars. *Journal of Analytical Atomic Spectrometry*, 31(4), 863–889. <https://doi.org/10.1039/C5JA00417A>
- Milliken, R. E., Grotzinger, J. P., & Thomson, B. J. (2010). Paleoclimate of Mars as captured by the stratigraphic record in Gale Crater. *Geophysical Research Letters*, 37(4), L04201. <https://doi.org/10.1029/2009GL041870>
- Milliken, R. E., & Mustard, J. F. (2005). Quantifying absolute water content of minerals using near-infrared reflectance spectroscopy. *Journal of Geophysical Research*, 110(E12), E12001. <https://doi.org/10.1029/2005JE002534>
- Morrison, S. M., Downs, R. T., Blake, D. F., Prabhu, A., Eleish, A., Vaniman, D. T., et al. (2018). Relationships between unit-cell parameters and composition for rock-forming minerals on Earth, Mars, and other extraterrestrial bodies. *American Mineralogist*, 103(6), 848–856. <https://doi.org/10.2138/am-2018-6123>

- Morrison, S. M., Downs, R. T., Blake, D. F., Vaniman, D. T., Ming, D. W., Hazen, R. M., et al. (2018). Crystal chemistry of martian minerals from Bradbury landing through Naukluft Plateau, Gale crater, Mars. *American Mineralogist*, *103*(6), 857–871. <https://doi.org/10.2138/am-2018-6124>
- Newman, C. E., Gómez-Elvira, J., Marin, M., Navarro, S., Torres, J., Richardson, M. L., et al. (2017). Winds measured by the rover environmental monitoring station (REMS) during the Mars science laboratory (MSL) rover's Bagnold Dunes Campaign and comparison with numerical modeling using MarsWRF. *Icarus*, *291*, 203–231. <https://doi.org/10.1016/j.icarus.2016.12.016>
- Palucis, M. C., Dietrich, W. E., Williams, R. M. E., Hayes, A. G., Parker, T., Sumner, D. Y., et al. (2016). Sequence and relative timing of large lakes in Gale crater (Mars) after the formation of Mount Sharp. *Journal of Geophysical Research: Planets*, *121*(3), 472–496. <https://doi.org/10.1002/2015JE004905>
- Peterson, R. C., & Wang, R. (2006). Crystal molds on Mars: Melting of a possible new mineral species to create martian chaotic terrain. *Geology*, *34*(11), 957–960. <https://doi.org/10.1130/G22678A.1>
- Rampe, E. B., Blake, D. F., Bristow, T. F., Ming, D. W., Vaniman, D. T., Morris, R. V., et al. (2020). Mineralogy and geochemistry of sedimentary rocks and eolian sediments in Gale crater, Mars: A review after six Earth years of exploration with Curiosity. *Geochemistry*, *80*(2), 125605. <https://doi.org/10.1016/j.chemer.2020.125605>
- Rapin, W., Bousquet, B., Lasue, J., Meslin, P.-Y., Lacour, J.-L., Fabre, C., et al. (2017). Roughness effects on the hydrogen signal in laser-induced breakdown spectroscopy. *Spectrochimica Acta Part B: Atomic Spectroscopy*, *137*, 13–22. <https://doi.org/10.1016/j.sab.2017.09.003>
- Rapin, W., Dromart, G., Rubin, D., Deit, L. L., Mangold, N., Edgar, L. A., et al. (2021). Alternating wet and dry depositional environments recorded in the stratigraphy of Mount Sharp at Gale crater, Mars. *Geology*, *49*(7), 842–846. <https://doi.org/10.1130/G48519.1>
- Rapin, W., Ehlmann, B. L., Dromart, G., Schieber, J., Thomas, N. H., Fischer, W. W., et al. (2019). An interval of high salinity in ancient Gale Crater Lake on Mars. *Nature Geoscience*, *12*(11), 889–895. <https://doi.org/10.1038/s41561-019-0458-8>
- Rapin, W., Meslin, P.-Y., Maurice, S., Wiens, R. C., Laporte, D., Chauviré, B., et al. (2017). Quantification of water content by laser induced breakdown spectroscopy on Mars. *Spectrochimica Acta Part B: Atomic Spectroscopy*, *130*, 82–100. <https://doi.org/10.1016/j.sab.2017.02.007>
- Rodríguez, A., & Van Bergen, M. J. (2016). Volcanic hydrothermal systems as potential analogues of martian sulphate-rich terrains. *Netherlands Journal of Geosciences*, *95*(2), 153–169. <https://doi.org/10.1017/njg.2015.12>
- Sarrazin, P., Chipera, S., Bish, D., Blake, D., & Vaniman, D. (2005). Vibrating sample holder for XRD analysis with minimal sample preparation. *Advances in X-Ray Analysis*, *48*, 156–164.
- Savijärvi, H., McConnochie, T. H., Harri, A. M., & Paton, M. (2019). Annual and diurnal water vapor cycles at Curiosity from observations and column modeling. *Icarus*, *319*, 485–490. <https://doi.org/10.1016/j.icarus.2018.10.008>
- Sebastián, E., Armiens, C., Gómez-Elvira, J., Zorzano, M. P., Martínez-Frías, J., Esteban, B., & Ramos, M. (2010). The rover environmental monitoring station ground temperature sensor: A pyrometer for measuring ground temperature on Mars. *Sensors*, *10*, 9211–9231. <https://doi.org/10.3390/s101009211>
- Sheppard, R. Y., Milliken, R. E., Parente, M., & Itoh, Y. (2021). Updated perspectives and hypotheses on the mineralogy of lower Mt. Sharp, Mars, as seen from orbit. *Journal of Geophysical Research: Planets*, *126*(2), e2020JE006372. <https://doi.org/10.1029/2020JE006372>
- Smith, R. J., McLennan, S. M., Sutter, B., Rampe, E. B., Dehouck, E., Siebach, K. L., et al. (2022). X-Ray amorphous sulfur-bearing phases in sedimentary rocks of Gale crater, Mars. *Journal of Geophysical Research: Planets*, *127*(5), e2021JE007128. <https://doi.org/10.1029/2021JE007128>
- Smith, R. J., Rampe, E. B., Horgan, B. H. N., & Dehouck, E. (2018). Deriving amorphous component abundance and composition of rocks and sediments on Earth and Mars. *Journal of Geophysical Research: Planets*, *123*(10), 2485–2505. <https://doi.org/10.1029/2018JE005612>
- Steiger, M., Linnow, K., Ehrhardt, D., & Rohde, M. (2011). Decomposition reactions of magnesium sulfate hydrates and phase equilibria in the $\text{MgSO}_4\text{-H}_2\text{O}$ and $\text{Na}^+\text{-Mg}^{2+}\text{-Cl}^- \text{-SO}_4^{2-}\text{-H}_2\text{O}$ systems with implications for Mars. *Geochimica et Cosmochimica Acta*, *75*(12), 3600–3626. <https://doi.org/10.1016/j.gca.2011.03.038>
- Thorpe, M. T., Bristow, T. F., Rampe, E. B., Tosca, N. J., Grotzinger, J. P., Bennett, K. A., et al. (2022). Mars Science Laboratory CheMin data from the Glen Torridon region and the significance of lake-groundwater interactions in interpreting mineralogy and sedimentary history. *Journal of Geophysical Research: Planets*, *127*(11), e2021JE007099. <https://doi.org/10.1029/2021JE007099>
- Toner, J. D., Catling, D. C., & Light, B. (2014). The formation of supercooled brines, viscous liquids, and low-temperature perchlorate glasses in aqueous solutions relevant to Mars. *Icarus*, *233*, 36–47. <https://doi.org/10.1016/j.icarus.2014.01.018>
- Tosca, N. J., McLennan, S. M., Clark, B. C., Grotzinger, J. P., Hurowitz, J. A., Knoll, A. H., et al. (2005). Geochemical modeling of evaporation processes on Mars: Insight from the sedimentary record at Meridiani Planum. *Earth and Planetary Science Letters*, *240*(1), 122–148. <https://doi.org/10.1016/j.epsl.2005.09.042>
- Vaniman, D. T., Bish, D. L., Chipera, S. J., Fialips, C. I., Carey, J. W., & Feldman, W. C. (2004). Magnesium sulphate salts and the history of water on Mars. *Nature*, *431*(7009), 663–665. <https://doi.org/10.1038/nature02973>
- Vaniman, D. T., & Chipera, S. J. (2006). Transformation of Mg- and Ca-sulfate hydrates in Mars regolith. *American Mineralogist*, *91*(10), 1628–1642. <https://doi.org/10.2138/am.2006.2092>
- Vaniman, D. T., Chipera, S. J., Bish, D. L., & Peterson, R. C. (2007). Mars latitude, Mars obliquity, and hydration states of Mg-Sulfates. In *7th international conference on Mars*. Abstract #3156.
- Vaniman, D. T., Martínez, G. M., Rampe, E. B., Bristow, T. F., Blake, D. F., Yen, A. S., et al. (2018). Gypsum, bassanite, and anhydrite at Gale crater, Mars. *American Mineralogist*, *103*(7), 1011–1020. <https://doi.org/10.2138/am-2018-6346>
- Wang, A., Freeman, J. J., Chou, I.-M., & Jolliff, B. L. (2011). Stability of Mg-sulfates at -10°C and the rates of dehydration/rehydration processes under conditions relevant to Mars. *Journal of Geophysical Research*, *116*(E12), E12006. <https://doi.org/10.1029/2011JE003818>
- Wang, A., Freeman, J. J., & Jolliff, B. L. (2007). Formation rate of amorphous magnesium sulfates at low temperatures approaching the current surface conditions on Mars. *Lunar and Planetary Science Conference, XXXVIII*. Abstract 1195.
- Wang, A., Freeman, J. J., & Jolliff, B. L. (2009). Phase transition pathways of the hydrates of magnesium sulfate in the temperature range 50°C to 5°C : Implication for sulfates on Mars. *Journal of Geophysical Research*, *114*(E4), E04010. <https://doi.org/10.1029/2008JE003266>